

MEASUREMENT OF THE VERTICAL EMITTANCE AND β -FUNCTION AT THE PEP-II INTERACTION POINT USING THE BABAR DETECTOR*

J. M. Thompson[†], A. Roodman, Stanford Linear Accelerator Center, Menlo Park, CA 94025, U. S. A.
W. Kozanecki, DAPNIA-SPP, CEA-Saclay, 91191 Gif-sur-Yvette, France

Abstract

We present measurements of the effective vertical emittance and IP β -function in the PEP-II asymmetric B Factory at SLAC. These beam parameters are extracted from fits to the longitudinal dependence of the luminosity and the vertical luminous size, measured using $e^+e^- \rightarrow \mu^+\mu^-$ events recorded in the *BABAR* detector. The results are compared, for different sets of machine conditions, to accelerator-based measurements of the optical functions of the two beams.

INTRODUCTION

Maximizing the luminosity at colliding beam storage rings requires knowledge and control of the ring optics and beam conditions. In this paper we present measurements of the vertical β -functions and emittances of the PEP-II asymmetric storage rings at SLAC using measurements from the *BABAR* detector.

PEP-II consists of two rings, a high-energy-ring (HER) storing 9.0 GeV electrons and a low-energy-ring (LER) storing 3.1 GeV positrons [1]. The HER and LER have independent β -functions and emittances. The so-called “hourglass effect” arises from the non-zero angular divergence of the beams at the interaction point (IP), and becomes significant in the vertical (y) direction, where the IP β -function is comparable in size to the longitudinal (z) width of the luminous region. The β -function near the IP for beam $i = \text{HER, LER}$ is

$$\beta_{i,y}(z) = \beta_{i,y}^* \left(1 + \frac{(z - z_{i,0})^2}{\beta_{i,y}^{*2}} \right), \quad (1)$$

where $z_{i,0}$ is the location of the “waist” where the β -function reaches its minimum value $\beta_{i,y}^*$. The Gaussian width of a single beam i is given by

$$\sigma_{i,y}(z) = \sqrt{\varepsilon_{i,y} \beta_{i,y}(z)}, \quad (2)$$

where $\varepsilon_{i,y}$ is the vertical emittance of that beam.

The dimensions of the luminous region are calculated from the overlap integral of the single beam distributions. The resulting vertical width is

$$\sigma_y^L(z) = (1/\sigma_{\text{HER},y}^2 + 1/\sigma_{\text{LER},y}^2)^{-1/2}. \quad (3)$$

The longitudinal distribution of the luminosity is given by

*Work supported in part by DOE Contract DE-AC02-76SF00515

[†]joshmt@slac.stanford.edu

$$\frac{d\mathcal{L}}{dz} = \frac{\mathcal{L}_0}{\Sigma_x \Sigma_y} \exp \left(-\frac{1}{2} \frac{(z - z_c)^2}{(\Sigma_z/2)^2} \right), \quad (4)$$

where z_c is the centroid of the luminous region and the width Σ_z depends on the bunch lengths of the beams. The shape is modified from a Gaussian by the factors

$$\Sigma_j = \sqrt{\varepsilon_{\text{HER},j} \beta_{\text{HER},j}(z) + \varepsilon_{\text{LER},j} \beta_{\text{LER},j}(z)}, \quad (5)$$

where $j = x, y$. Note that the z -dependence of Σ_x is negligible because β_x^* is large. \mathcal{L}_0 is a constant [2].

The longitudinal dependence of the vertical size of the luminous region and the longitudinal distribution of luminosity were first used to extract beam parameters by Cinabro *et al.*, using the CLEO detector at CESR [3]. The authors find that the detector resolution is constant in z , and perform a simultaneous fit to eqs. 3 and 4 to extract β_y^* , ε_y , and the resolution. We introduce a technique in which detector resolution estimates for each event are used in conjunction with the resolution as measured in the data, allowing vertical IP β -functions and emittances to be extracted from the measurement of $\sigma_y^L(z)$ alone. The measurement of the $d\mathcal{L}/dz$ distribution can then provide an independent measurement of the IP β -functions.

METHOD

The two muons in each event are reconstructed independently. Loose selection cuts are applied to remove backgrounds such as cosmic rays and events with poorly reconstructed tracks.

All reconstruction is performed in a coordinate system where the z axis is aligned with that of the luminous region and the origin lies at its centroid, as determined by a calibration performed every 10 minutes during data taking [4]. The reconstructed quantities are shown schematically in Figure 1. For each track, the reconstruction algorithm determines the point of closest approach (poca) to the beam axis. The distance in the x - y plane from the poca to the origin is the distance of closest approach (doса) for the track. The doса sign depends on the track direction. The reconstruction algorithm estimates the uncertainty on the doса, $\delta_{\text{doса}}$, using a sophisticated model of the detector to take into account the interactions between the particle and the detector material. The z coordinate of each track is taken to be the z at the poca. Additionally, each track has an azimuthal angle ϕ measured from the x -axis, and a dip angle λ measured from the x - y plane [5].

For the measurement of $\sigma_y^L(z)$, the analysis strategy is to estimate the event origin using the simple mean of the

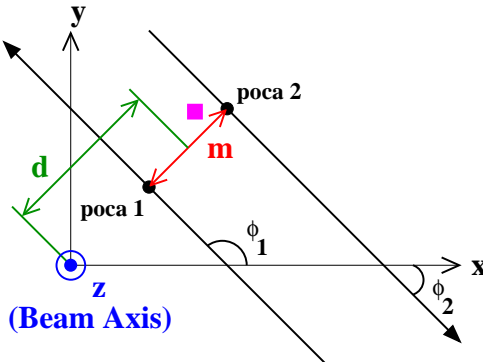


Figure 1: Schematic view of two reconstructed muon tracks, where the square indicates the hypothetical true production point. Each track has a point of closest approach (poca) to the beam axis, from which average doca (d) and miss distance (m) are calculated. The azimuthal angles (ϕ_1, ϕ_2) measure the x - y orientation of the tracks.

track docas, d . For each event we choose one of the two ϕ 's at random and construct a weighted average of the z measurements. These parameters are the observables in a Gaussian probability density function (PDF),

$$\mathcal{P}(d, \phi) = \exp\left(-\frac{1}{2} \frac{d^2}{\sigma_y^L \cos^2 \phi + \sigma_x^L \sin^2 \phi}\right), \quad (6)$$

which incorporates the beam parameters through σ_y^L as defined in equation 3. The parameters σ_x^L and σ_y^L describe the Gaussian widths of the transverse luminous distributions. By using the angle ϕ , this PDF extracts maximal information about x and y from the observable d .

We define the quantity miss distance, m , designed to be sensitive to track resolution only, as the difference between the track docas. Since both d and m are linear combinations of the track docas, the estimated error on both is proportional to the quadrature sum of the track doca errors, $\delta = \sqrt{\delta_{doca,1}^2 + \delta_{doca,2}^2}$.

Resolution Model

The estimated error on the track doca varies from 15 μm to 30 μm depending on the details of the track's trajectory in the detector. Additionally, the average detector resolution is correlated with, for example, the z coordinate of the track, varying by about 10% over the range of z . To account for these variations, for each event we use the quantity δ to provide an estimate of the resolution which takes into account the particular geometry of the tracks. The miss distance m , aggregated over many events, provides a direct measurement of the resolution. We introduce a resolution function, $\mathcal{R}(m; \delta)$, to reconcile the estimated error δ with the measured resolution. This function is parameterized as the sum of three Gaussian distributions, a core distribution with a narrow width and two wider distributions to account for non-Gaussian tails.

Fit Procedure

Our results are extracted from a sequence of unbinned maximum likelihood (ML) fits and binned fits. We perform a ML fit to the resolution function \mathcal{R} first, fix the resolution parameters, and fit for the transverse luminous sizes using eq. 6. To account for variation in the resolution corrections, some resolution parameters are refit in bins of z . Subsequently, a series of fits to the PDF \mathcal{P} is performed in bins of z to extract the z -dependence of σ_y^L . Finally, the beam parameters are extracted from a binned χ^2 fit to eq. 3.

For the fit to the $d\mathcal{L}/dz$ distribution, we form a PDF directly from equation 4. As discussed in the following section, fits to the observable z are used to extract Σ_z , z_c , and the z -dependence of Σ_y .

Validation

The fit to the vertical size of the luminous region is validated using samples of simulated events, generated in the GEANT-based BABAR Monte Carlo (MC) [6] with simple Gaussian distributions for the luminous region, ignoring the hourglass effect. We perform test fits to 10 samples, generated with σ_y^L from 2 μm to 20 μm , where the expected physical value is about 3 μm . Fitting the results to the function $\sigma_{y,\text{fit}}^L = \sqrt{\sigma_{y,\text{generated}}^L{}^2 + \sigma_{y,\text{bias}}^L{}^2}$, a bias $\sigma_{y,\text{bias}}^L$ on the value of σ_y^L of $2.0 \pm 0.3 \mu\text{m}$ is extracted. This bias is not observed in fits to data samples generated directly from the PDF. In the nominal fits to data, we account for this bias by adding it in quadrature in the PDF. To test the entire fit procedure, a fit is performed to a MC sample generated according to equations 1-5. For generated parameters $\beta_y^* = 1.3 \text{ cm}$ and $\varepsilon_{y,\text{eff}} = 1.2 \text{ nm} \cdot \text{rad}$ (see eq. 7), the fit returns $\beta_y^* = 1.6 \pm 0.2 \text{ cm}$ and $\varepsilon_{y,\text{eff}} = 1.6 \pm 0.2 \text{ nm} \cdot \text{rad}$.

With sufficient statistics, the fit to the longitudinal distribution of luminosity shows no significant bias when fitting to samples generated from the PDF. A fit to the hourglass MC sample gives results compatible with the generated values. We confirm that the detector efficiency is constant as a function of z .

RESULTS

To reduce the number of free parameters in the fits, we make several assumptions. The β -functions for the HER and LER are assumed to be identical ($\beta_y^* = \beta_{\text{HER},y}^* = \beta_{\text{LER},y}^*$), and we assume the magnetic waists are aligned with the bunch crossing point ($z_{0,\text{HER}} = z_{0,\text{LER}} = z_c$). In the fit to the vertical luminous size, we extract an effective vertical emittance,

$$\varepsilon_{y,\text{eff}} = 2 \frac{\varepsilon_{\text{HER},y} \varepsilon_{\text{LER},y}}{\varepsilon_{\text{HER},y} + \varepsilon_{\text{LER},y}}. \quad (7)$$

Results of a sample fit to $\sigma_y^L(z)$ are shown in Fig. 2. In addition to the assumptions listed above, z_c is fixed to zero in this fit, leaving β_y^* and $\varepsilon_{y,\text{eff}}$ floating in the binned fit.

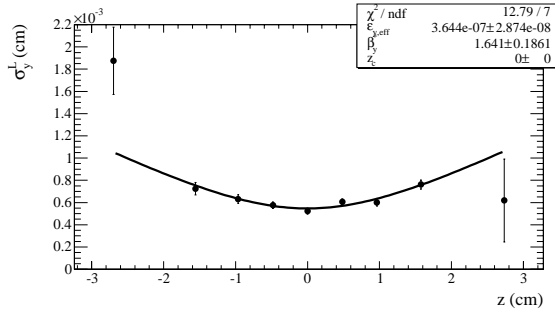


Figure 2: Results of a $\sigma_y^L(z)$ fit to the beam parameters. The points are the results of ML fits to σ_y^L in bins of z , and the curve is the best fit to eq. 3 using the the assumptions discussed in the text and fixing $z_c = 0$. All values shown are in cm.

For fits to the $d\mathcal{L}/dz$ distribution, data samples are divided such that each has a constant RF voltage for both rings. A sample fit to data is shown in Fig. 3.

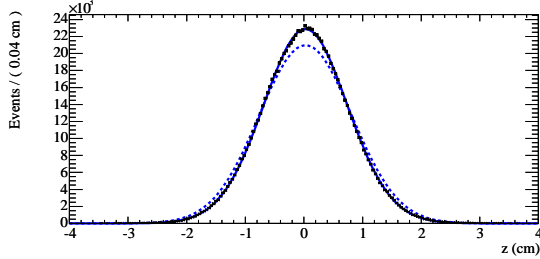


Figure 3: The solid curve is the $d\mathcal{L}/dz$ curve for a fit to a data z distribution (points). The dashed curve is a Gaussian distribution with width $\Sigma_z/2$.

Figures 4 and 5 summarize the results of fits to data samples spanning the duration of “Run 4” of PEP-II operations, from September 2003 through July 2004. Fig. 4 shows β_y^* results from both $\sigma_y^L(z)$ and $d\mathcal{L}/dz$ fits, with a comparison to values taken from phase advance measurements [7]. For the $d\mathcal{L}/dz$ fits, the $\chi^2/\text{d.o.f.}$ values range from about 0.5 to 2 for 200 bins, and fits with fewer than 100000 events are not shown due to a possible fit bias. Results for the effective vertical emittance are shown in Fig. 5.

Systematic Effects

For the $\sigma_y^L(z)$ results, the bias correction is strongly correlated with the measured parameters. An underestimate of this correction will result in overestimates of both $\varepsilon_{y,\text{eff}}$ and β_y^* . In the fits to the $d\mathcal{L}/dz$ distribution, there is a complete anti-correlation between the results for Σ_z and β_y^* . Changes in the bunch lengths can thus bias the β_y^* result.

CONCLUSION

Using the *BABAR* detector, two independent techniques are used to measure the value of β_y^* for the PEP-II storage

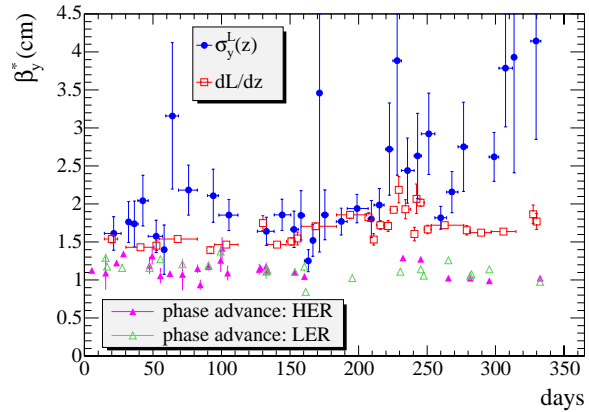


Figure 4: β_y^* as a function of time, from September 2003 through July 2004. Closed circles: $\sigma_y^L(z)$ fits; Open squares: $d\mathcal{L}/dz$ fits; Closed triangles: phase advance measurements of $\beta_{HER,y}^*$; Open triangles: phase advance measurements of $\beta_{LER,y}^*$. Two consecutive bins between 280 and 300 days, with values $\beta_y^* = 20 \pm 9$ cm and $\beta_y^* = 10 \pm 14$ cm, are excluded from the plot.

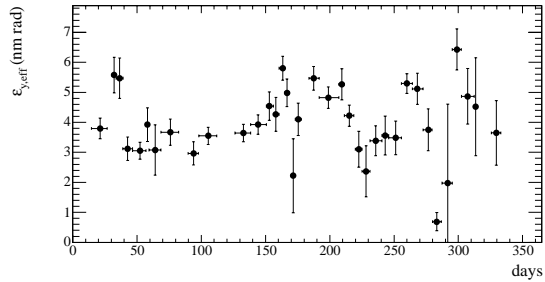


Figure 5: $\varepsilon_{y,\text{eff}}$ as a function of time, from September 2003 through July 2004.

rings as a fuction of time. Particularly for later times, there is a discrepancy between these measurements and values from accelerator phase advance measurements. Similar results are presented in Ref. [4]. Additionally, by directly measuring the detector resolution in data and accounting for it in a detailed model, measurements of $\sigma_y^L(z)$ are used to extract the effective vertical emittance.

REFERENCES

- [1] J. Seeman *et al.*, PAC’05, these proceedings (TPPP035).
- [2] M. Venturini and W. Kozanecki, SLAC-PUB-8699.
- [3] D. Cinabro *et al.*, Nucl. Instrum. Meth. A **481**, 29 (2002).
- [4] B. F. Viaud *et al.*, PAC’05, these proceedings (TPAT076).
- [5] B. Aubert *et al.* [BABAR Collaboration], Nucl. Instrum. Meth. A **479**, 1 (2002).
- [6] S. Agostinelli *et al.* [GEANT4 Collaboration], Nucl. Instrum. Meth. A **506**, 250 (2003).
- [7] G. Yocky, Private communication.